remote sensing

MDPI

Technical Note

Monitoring and Predicting the Subsidence of Dalian Jinzhou Bay International Airport, China by Integrating InSAR Observation and Terzaghi Consolidation Theory

Xianlin Shi [1], Chen Chen [1], Keren Dai [1,2,*], Jin Deng [1], Ningling Wen [1], Yong Yin [1] and Xiujun Dong [2]

[1] College of Earth Science, Chengdu University of Technology, Chengdu 610059, China; shixianlin06@cdut.edu.cn (X.S.); chenchen1@stu.cdut.edu.cn (C.C.); dengjin@stu.cdut.edu.cn (J.D.); wenningling@stu.cdut.edu.cn (N.W.); yinyong@stu.cdut.edu.cn (Y.Y.)

[2] State Key Laboratory of Geological Disaster Prevention and Geological Environmental Protection, Chengdu University of Technology, Chengdu 610059, China; dongxiujun@cdut.cn

* Correspondence: daikeren17@cdut.edu.cn

Abstract: Dalian Jinzhou Bay International Airport (DJBIA) is an offshore artificial island airport, where the reclaimed land is prone to uneven land subsidence due to filling consolidation and construction. Monitoring and predicting the subsidence are essential to assist the subsequent subsidence control and ensure the operational safety of DJBIA. However, the accurate monitoring and prediction of reclaimed subsidence for such a wide area under construction are hard and challenging. This paper utilized the Small Baseline Subset Synthetic Aperture Radar (SBAS-InSAR) technology based on Sentinel-1 images from 2017 to 2021 to obtain the subsidence over the land reclamation area of the DJBIA, in which the results from ascending and descending orbit data were compared to verify the reliability of the results. The SBAS-InSAR results reveal that uneven subsidence is continuously occurring, especially on the runway, terminal, and building area of the airport, with the maximum subsidence rate exceeding 100 mm/year. It was found that there is a strong correlation between the subsidence rate and backfilling time. This study provides important information on the reclaimed subsidence for DJBIA and demonstrates a novel method for reclaimed subsidence monitoring and prediction by integrating the advanced InSAR technology and Terzaghi Consolidation Theory modeling. Moreover, based on the Terzaghi consolidation theory and the corresponding geological parameters of the airport, predicted subsidence curves in this area are derived. The comparison between predicted curves and the actual subsidence revealed by InSAR in 2017–2021 is highly consistent, with a similar trend and falling in a range of ±25 mm/year, which verifies that the subsidence in this area conforms to Terzaghi Consolidation Theory. Therefore, it can be predicted that in the future, the subsidence rate of the new reclamation area in this region will reach about 80 mm/year ± 25 mm/year, and the subsidence rate will gradually slow down with the accumulation of reclamation time. The subsidence rate will slow down to about 30 mm/year ± 25 mm/year after 10 years.

Keywords: Dalian Jinzhou Bay International Airport; SBAS-InSAR; Terzaghi consolidation theory; subsidence monitoring; subsidence prediction

Citation: Shi, X.; Chen, C.; Dai, K.; Deng, J.; Wen, N.; Yin, Y.; Dong, X. Monitoring and Predicting the Subsidence of Dalian Jinzhou Bay International Airport, China by Integrating InSAR Observation and Terzaghi Consolidation Theory. *Remote Sens.* **2022**, *14*, 2332. https://doi.org/10.3390/rs14102332

Academic Editors: Chisheng Wang, Daqing Ge, Guohong Zhang, Wu Zhu and Siting Xiong

Received: 2 April 2022
Accepted: 3 May 2022
Published: 11 May 2022

1. Introduction

Dalian Jinzhou Bay International Airport (DJBIA), constructed in 2010, is built on a reclaimed artificial island with an overall planned reclamation area of 20.87 km^2, and all the reclaimed land will be used for the airport, which will be the largest offshore airport worldwide after construction. Land reclamation is prone to unstable geological foundations due to sediment consolidation [1–4]. Airports built on reclaimed land commonly suffer from land subsidence, which will threaten the operational safety of the airport, especially the land subsidence occurring in runway areas [5]. Therefore, it is essential to monitor and

predict the ground subsidence in this area and assess its impact on the safe operation of the airport.

Reliable surface deformation information can be obtained through traditional point-measurement methods, such as level surveys or global satellite navigation and positioning technology. However, traditional measurement methods was difficult to apply them to ground subsidence monitoring at airports under reclamation. Interferometric synthetic aperture radar (InSAR) is an emerging geodetic technology. It is capable of acquiring high-accuracy and continuously covered surface deformation information, which is widely used in the fields of ground subsidence monitoring [1,3,6,7], and landslide monitoring [8–12]. In recent years, InSAR technology has been widely used in land subsidence monitoring at airports. Such as Hong Kong Chek Lap Kok Airport [13,14], Shanghai Pudong International Airport [15,16], Beijing Capital International Airport [17,18], Shenzhen Baoan International Airport [19,20], Kuala Lumpur International Airport, Malaysia [5], and Japanese airports [21–23]. The land formed by the land reclamation airport is characterized by high compressibility, low strength, and a large porosity ratio, which easily leads to ground subsidence. Studies related to reclaimed land airport monitoring by InSAR have been performed. Lu et al. [19] and Xu et al. [24] monitored ground subsidence at Shenzhen Baoan International Airport based on the SAR data from 2007 to 2010 and 2015 to 2019, revealing that the subsidence in the reclamation area was greater than in the ground, and dynamic loads is an important factor that causing airport subsidence. Zhuo et al. [25] conducted subsidence monitoring of Xiamen Xiang'an New Airport based on SBAS-InSAR from 2018 to 2020 and identified the areas that may be affected in the future based on the type of airport land use. Hong Kong Chek Lap Kok Airport [14] and Xiamen New Airport [26] used SAR data and geological data combined with Terzaghi consolidation theory for long-term subsidence monitoring of the reclamation airports. The above studies used InSAR observation on reclaimed airport subsidence monitoring and made a detailed analysis of subsidence. Integration of InSAR observation and geological condition of the artificial land area to predict the subsidence trend deserves further study.

In this paper, SBAS-InSAR was used to monitor the land subsidence at DJBIA based on 50 Sentinel-1A ascending SAR images between March 2017 and April 2021. The SABS-InSAR monitoring results reveal the regional distribution and time–series characteristics of airport subsidence. Based on the Terzaghi consolidation theory, the geological data of the airport were used to calculate the deformation of the soil layer at any time during the land reclamation process and to predict the subsidence development trend. The InSAR results verified that the subsidence in 2017–2021 is consistent with the predicted curve of the Terzaghi consolidation theory in the area. The integration of InSAR observation and Terzaghi Consolidation Theory works well in this area and could make a great contribution to the subsidence prediction.

2. Study Area and Data Source

2.1. Study Area

Dalian, in Liaoning Province (China), is located between the Yellow Sea and the Bohai Sea, surrounded by the sea, and dominated by mountainous and hilly peninsular landforms. The hills are northeast-southwest direction, with relatively flat terrain on the east and west sides [27]. The study area, DJBIA, is in the sea area of Jinzhou Bay, Dalian City. DJBIA is an offshore artificial island airport on the Chinese mainland, which consists of berms, the runway, and the building area (Figure 1). The western bay of Jinzhou District, where the airport is located, belongs to the high-risk area for geological disasters [28].

DJBIA can serve an average annual passenger throughput of 43 million and 550,000 tons of cargo and mail [29]. Its construction aims to effectively alleviate the tight operating resources and over-saturation of throughput at Dalian Zhoushuizi International Airport, and provide strong support for economic and social development and comprehensive transportation construction in Dalian. DJBIA has a total planned area of 20.87 km^2, including a terminal area of 500,000 m^2, with two 3600 m long teleparallel runways, 45 m, and 60 m

wide, respectively [29]. The airport started to fill the land from the beginning of 2010. To better analyze the characteristics of subsidence, the reclaimed area from 2010 to 2021 was defined as six reclamation stages with a period of every two years. The spatial distribution of the reclamation area and reclamation area in different stages is shown in Figure 2a. The road to the airport has been completed in 2011, the building area and part of the terminal in 2013, all of the terminal and part of the heliport filled in 2015, and the focus on the runway and building area filled from 2017 to 2021. As shown in Figure 2b, the largest increase in filled area was 4.96 km^2 in 2015 and the accumulation of filled area will reach 11.29 km^2 by April 2021.

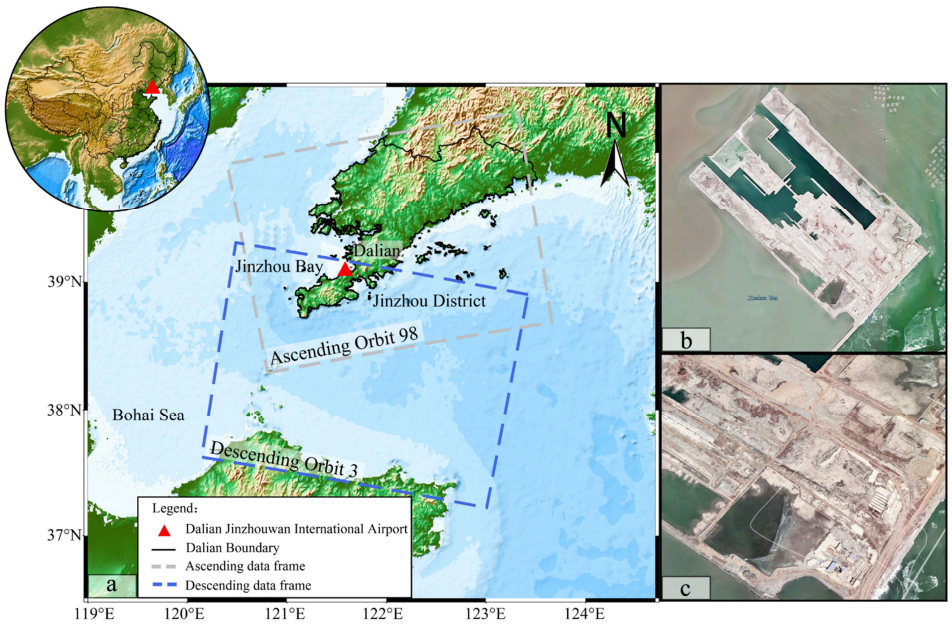

Figure 1. Overview of Dalian Jinzhou Bay International Airport: (**a**) Location of the study area; (**b**,**c**) Satellite map of the study area.

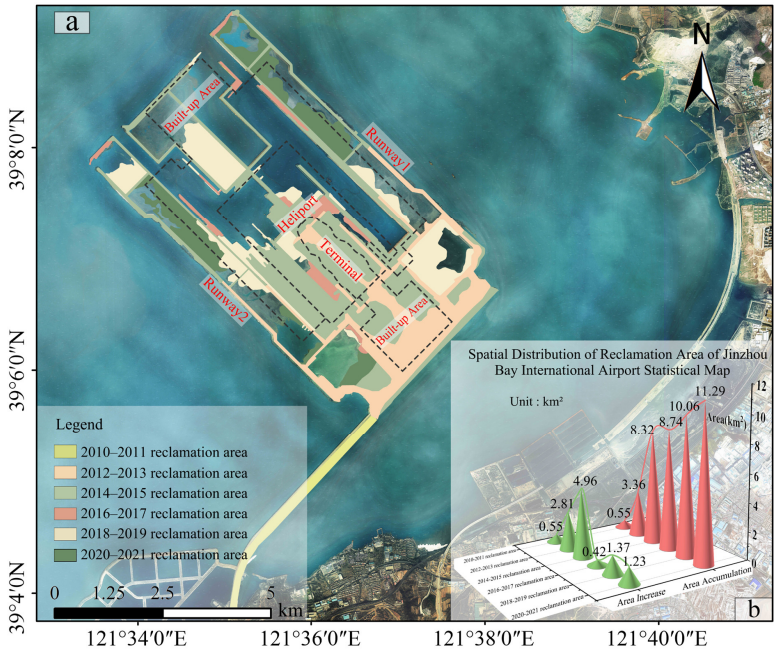

Figure 2. Spatial distribution of different reclamation stages: (**a**) Map of area change of the airport from 2011 to 2021; (**b**) Statistical of the increasement and accumulation of reclamation area. Reclamation data source: Google Earth.

2.2. Data Source

In this paper, 50 images of Sentinel-1A ascending orbit and 15 images of Sentinel-1B descending orbit from the European Space Agency (ESA) were acquired to monitor ground subsidence at DJBIA. The main obtained include orbit, resolution, polarization mode, and other parameter information, other detailed parameter information, as shown in Table 1. The 30 m resolution SRTM DEM data provided by the National Aeronautics and Space Administration (NASA) was used in the data processing, to remove the topographic phase. It is worth noting that the study area in this paper is a new reclamation area, and the airport area does not have the latest DEM in the SRTM data or other data. Considering that the entire area is relatively flat (the fluctuation is within 5 m) and the spatial baseline of the sentinel data is controlled within 100 m, the effect of elevation residuals on the deformation of relatively flat terrain in this case of short vertical baseline interference pairs can be neglected. Based on the 50 ascending images, a temporal baseline threshold of 100 days and a spatial baseline threshold of 221 m were set, and 132 pairs of interference pairs were generated by the combination (Figure 3). Spatial and temporal baselines of Sentinel-1 ascending and descending data are shown in Figure 3, Figure 4 respectively.

Table 1. Basic information of the Sentinel-1 images.

Parameter	Value	
Satellite	Sentinel-1A	Sentinel-1B
Orbit	Ascending	Descending
Azimuth/Range pixel spacing	13.99 m/2.33 m	13.99 m/2.33 m
Radar wavelength	5.6 cm	5.6 cm
Polarization mode	VV	VV
Revisit period	12 d	12 d
The angle of incidence	39.2°	39.1°
Temporal coverage	2017.03–2021.04	2019.12.20–2021.04.13
Number of images	50	15

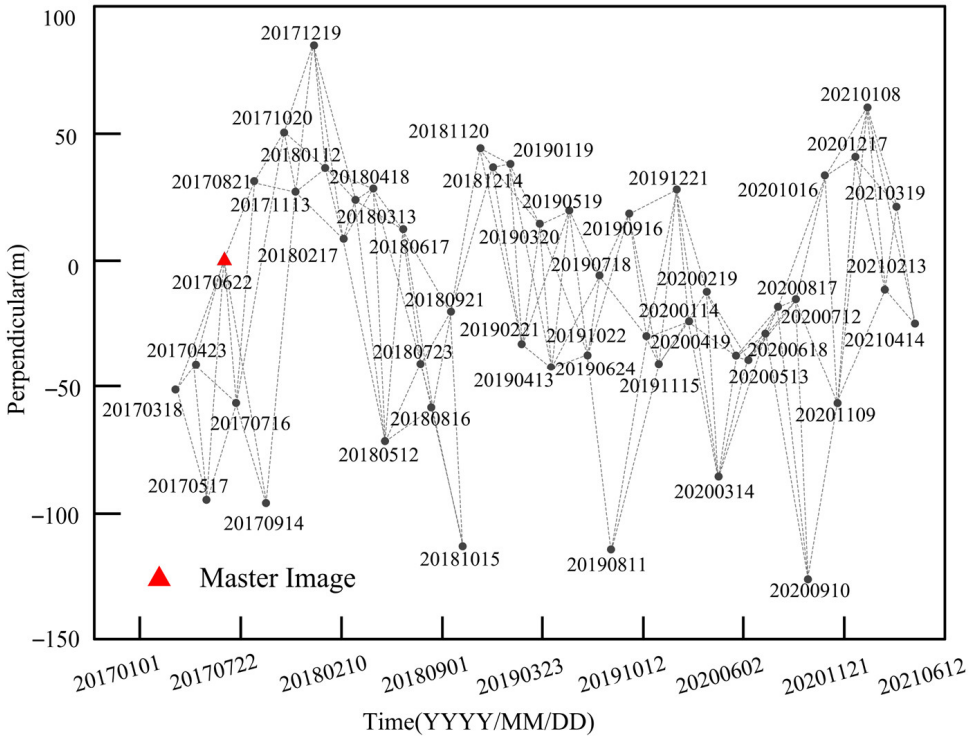

Figure 3. Spatial and temporal baselines of Sentinel-1 ascending data.

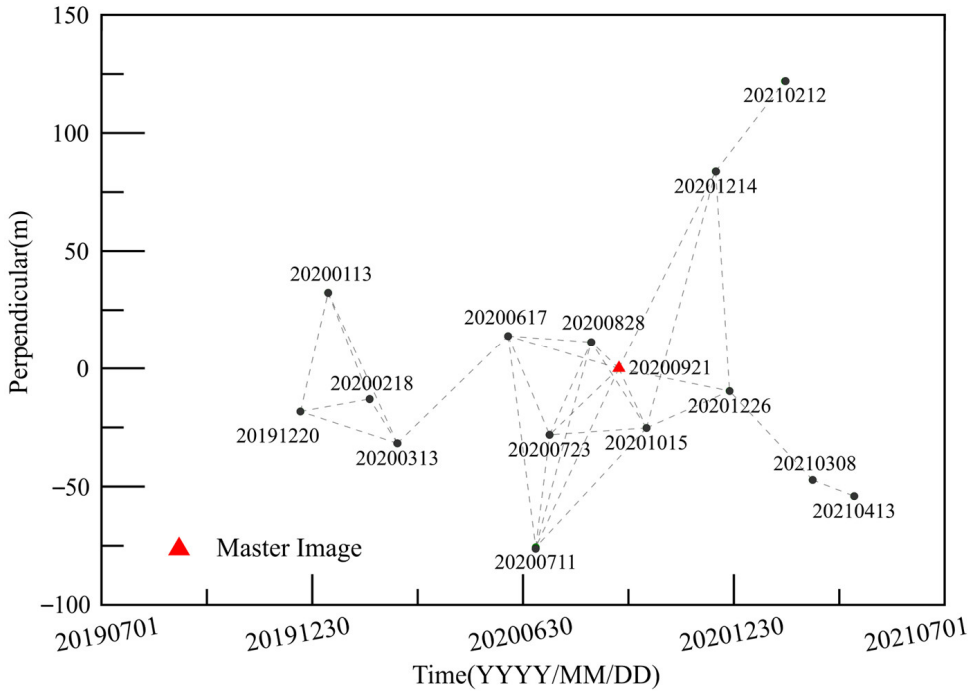

Figure 4. Spatial and temporal baselines of Sentinel-1 descending data.

DJBIA was reclaimed through rock excavation, and the major foundation filled in the site is soft soil, which can be approximately divided into highly compressible silt and clay [30,31]. This kind of foundation condition will result in large foundation subsidence. In order to calculate the subsidence of the reclamation area, geological parameters, such as initial pore ratio, compression coefficient, and the water gravity [30,32] were selected for further analysis in this paper. Detailed information is shown in Table 2.

Table 2. Experiment data in the airport.

Parameter	Corresponding Values
Permeability Coefficient	$\alpha = 0.0342$ m/year
Initial Porosity Ratio	$k_0 = 0.806$
Compression Coefficient	$\beta = 3.52 \times 10^{-4}$ kPa^{-1}
Water Gravity	$G_w = 10.101$ kN/m^3
Maximum Drainage Distance	H = −19.4 m
Solidification Stress	$\Gamma = 250$ kPa
Coefficient of Consolidation	C = 17.3959

3. Methodology

In this paper, the subsidence rate of the airport was firstly monitored based on SBAS-InSAR technology, and the subsidence prediction curve of the area was derived by combining the Terzaghi consolidation theory model with the geological sampling data of the airport. Then, the ground subsidence rate results were compared with the subsidence prediction curve to verify the applicability and accuracy of the prediction curve of the Terzaghi consolidation theory. Finally, the development trend of airport subsidence is determined based on this prediction curve. The detailed technology flow chart is shown in Figure 5.

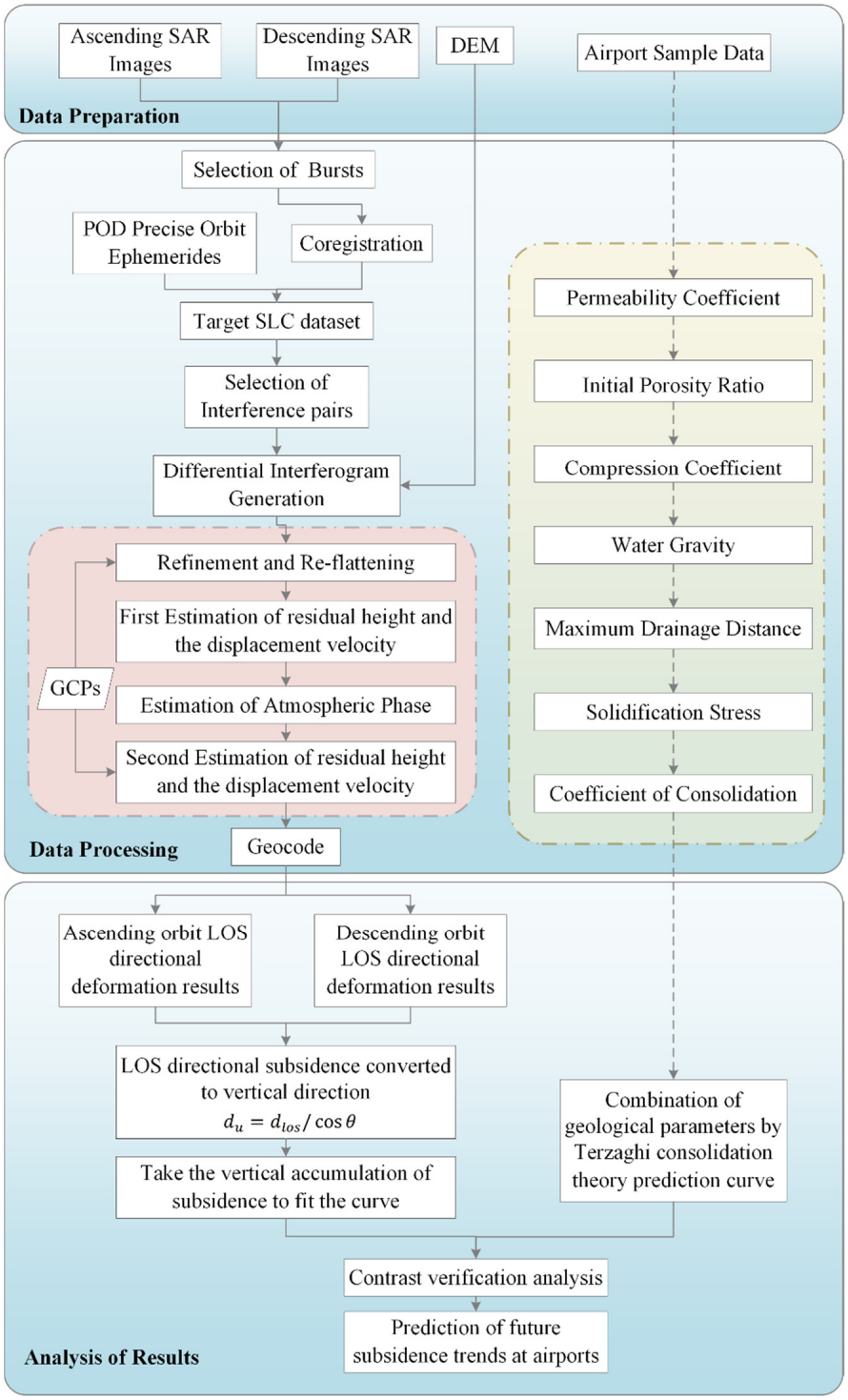

Figure 5. Flowchart of Integration of SBAS-InSAR and Terzaghi consolidation theory.

3.1. SBAS-InSAR Technology

In 2002, Berardino et al. proposed SBAS-InSAR as a novel technology with great prospects for application in the field of monitoring ground subsidence over long-term time series [33,34]. The technology has better applicability and reliability in areas of changing ground cover because it can reduce the negative effects of incoherence and DEM errors. To detect ground subsidence at the airport, the paper used the SBAS plug-in in ENVI software for step-by-step calculation. It includes three main steps: data pre-processing, interferogram generation, and deformation result generation.

The detailed steps of SBAS-InSAR technology are as follows:

Assuming that there are N +1 SAR images covering the same area acquired according to the time series, the image acquisition time series is:

$$t = [t_0, \ldots, t_N]^T \tag{1}$$

After selecting one of them as the master image for registration, in all the free combinations of differential interferometric pairs selected to meet the time baseline and spatial baseline thresholds, $\boldsymbol{M}$ differential interferograms can be obtained, then there are:

$$\frac{N+1}{2} \le M \le N\left(\frac{N+1}{2}\right) \tag{2}$$

Combined with the orbit data and external digital elevation model data to remove the flat and terrain effects. The noise is effectively removed by multi-viewing and filtering. In order to obtain the accumulation of deformation on the radar LOS (Line of Sight, LOS), the minimum cost flow (MCF) method is used to perform phase unwinding of M interferometric pairs [35,36]. Suppose that the jth differential interferogram is generated by acquiring the SAR image from the moment of image t_A and the main image t_B, then the corresponding phase unwrapping at any pixel point in the jth interferogram can be expressed as:

$$\delta\varphi^j = \varphi(t_B) - \varphi(t_A) \approx \delta\varphi^j_{def} + \delta\varphi^j_{topo} + \delta\varphi^j_{atm} + \delta\varphi^j_{noise} \tag{3}$$

where $\delta\varphi^j$ is the interference phase at the point; $\varphi(t_A)$ and $\varphi(t_B)$ are the phase values at t_A and t_B moments, respectively, with respect to the initial moment t_0; $\delta\varphi^j_{def}$, $\delta\varphi^j_{topo}$, $\delta\varphi^j_{atm}$, $\delta\varphi^j_{noise}$ indicate the phase difference caused by deformation phase (along with the radar LOS), terrain error, atmospheric delay, and noise, respectively. In order to enhance the accuracy of the deformation monitoring results in the study area, these error terms need to be effectively estimated and eliminated.

Firstly, by selecting more uniform Ground Control Points (Ground Control Points, GCPs) for orbit refinement and re-flattening, not only the orbit parameters can be corrected, but also the residual phase and phase jumps can be estimated and removed [37]. Then, the residual elevation and deformation rate are estimated based on the linear model, and the wrapping phase will be unwrapped twice [38]. Finally, the atmospheric phase is removed by spatial high-pass filtering and temporal low-pass filtering [39]. After removing the above error phase components, the time series deformation information in the LOS direction is obtained by the SVD method.

Due to SAR radar satellite side-view imaging, LOS displacement as a component of real displacement can be acquired [24]. When the horizontal displacement is much smaller than the vertical component, the LOS direction displacement is dominated by vertical subsidence [24,25,40]. As the airport region is relative flat and not like the mountainous area in the InSAR processing, based on the imaging geometry relationship, d_{los} can be converted to ground subsidence d_u based on the incidence angle θ [41], as in Equation (4):

$$d_u = d_{los} / \cos\theta \tag{4}$$

where d_u is the vertical displacement component; d_{los} is the LOS displacement; θ is the radar incidence angle.

3.2. Terzaghi Consolidation Theory

Terzaghi consolidation theory is commonly used to calculate the deformation of a saturated soil layer at any time during infiltration consolidation. The basic assumptions of consolidation theory are as follows: at the point when more than 80% of the pore volume in the soil is filled with water, the soil can be considered saturated although a small amount

of gas is present, it is mostly a closed [42]. To find the deformation of the saturated soil layer at any time during infiltration consolidation, the Terzaghi consolidation theory can be established to solve the problem. The Terzaghi theory of consolidation makes many simplifications and assumptions about the changing parameter conditions of the soil during consolidation. Firstly, the external load is applied to the soil instantaneously and at once, and remains constant throughout the consolidation process. Secondly, the soil and water do not produce compression deformation, and the soil compression is caused by drainage. Finally, parameters such as permeability coefficient α and compression coefficient β of the soil during consolidation remain constant during consolidation [30].

In this paper, based on the basic assumptions of the conventional Terzaghi consolidation theory, a differential unit soil body with a height of d_h in the soil body is taken for analysis. The volume compression of the soil is equal to the difference between the inflow and outflow of water from the unit body, which is used to establish the consolidation differential equilibrium equation. Additionally, used Darcy's law and the effective stress principle to solve the equation and obtained the differential equation of Terzaghi consolidation theory [43,44]. As shown in Equation (5):

$$C\frac{\partial^2 P_w}{\partial h^2} = \frac{\partial P_w}{\partial t} \tag{5}$$

where C is the coefficient of consolidation (m^2/year); P_w is pore water pressure (kPa); The coefficient of consolidation C and the degree of time consolidation D_c of the soil can be expressed by Equations (6) and (7):

$$C = \alpha\frac{1+k_0}{\beta G_w} \tag{6}$$

$$D_c = 1 - \frac{8e^{-\frac{\pi^2 C}{4H^2}}}{\pi^2} \tag{7}$$

where α is the permeability coefficient (m/year); k_0 is the initial porosity ratio; β is the compression coefficient (kPa^{-1}); G_w is the water gravity (kN/m^3) and H is the maximum drainage distance (m).

Determining and deriving the relevant parameters can calculate any time soil consolidation subsidence S_t(m) [45]. As shown in Equation (8):

$$S_t = D_c\frac{\beta}{1+k_0}\gamma H \tag{8}$$

where γ is the Solidification Stress (kPa).

After obtaining the subsidence prediction curves according to the above calculation method and geological parameters, they were compared with the ground subsidence results monitored by SBAS-InSAR technology. Finally, the curves were used to predict the rate and trend of subsidence in the study area.

4. Results and Discussion

4.1. Analysis of Spatial and Temporal Subsidence Characteristics of DJBIA

The subsidence rate maps of DJBIA were retrieved from the SAR data from March 2017 to April 2021 as shown in Figure 6a, where the negative value denotes the subsidence (i.e., the displacement was far away from the satellite) and the reference point (no subsidence) was chosen away from the reclamation area shown as a red point. Figure 7b–e shows the coherence coefficient, differential interferogram, distribution of elevation residuals, and the error map in the time-series processing, respectively. It can be seen that the area has a high coherence coefficient, a clear interferogram, and small residuals in the time series analysis (maximum less than 4 mm/year). Since the study area is under long-term construction and exploitation, special consideration needs to be given to the possible errors due to inaccurate

external elevation information. According to the demand of the landfill here, the elevation error is about 10 m. Based on the results of related studies [46] and the better baseline control of the sentinel data (all vertical baselines are less than 150 m), it is projected that this part of the elevation error will cause the deformation measurement error of interference pair to be less than 2 mm and can be further weakened during the time-series analysis. The inversion results of the elevation residuals in Figure 7d also shows that the elevation residuals of the airport building area, terminal, and heliport are small (between 0.3 and 3 m). Therefore, the measurement errors caused by elevation errors can be controlled. In addition, we introduced the descending orbit data for the same period (December 2019 to April 2021), where the descending orbit data are missing from June-November 2019. It can be found that the deformation results are highly consistent with the ascending orbit results regarding the spatial distribution (Figure 7a). In the runway end area, the number of effective monitoring points becomes more as the backfill progresses, and there is a partial normal decrease in the deformation magnitude. The comparison of the time-series residual results with the ascending and descending orbit results in Figure 6e confirms that the InSAR results of this study are reliable. In summary, the InSAR monitoring results have high accuracy. Because of the lack of data from the descending orbit, the results of the ascending orbit were used for subsequent analysis to ensure data integrity. Since the study area is dominated by vertical ground deformation with minimal horizontal deformation, the absence of horizontal deformation is assumed here to approximate the ascending orbit deformation results to ground subsidence, which is convenient for subsequent 5-year long time series analysis and model building.

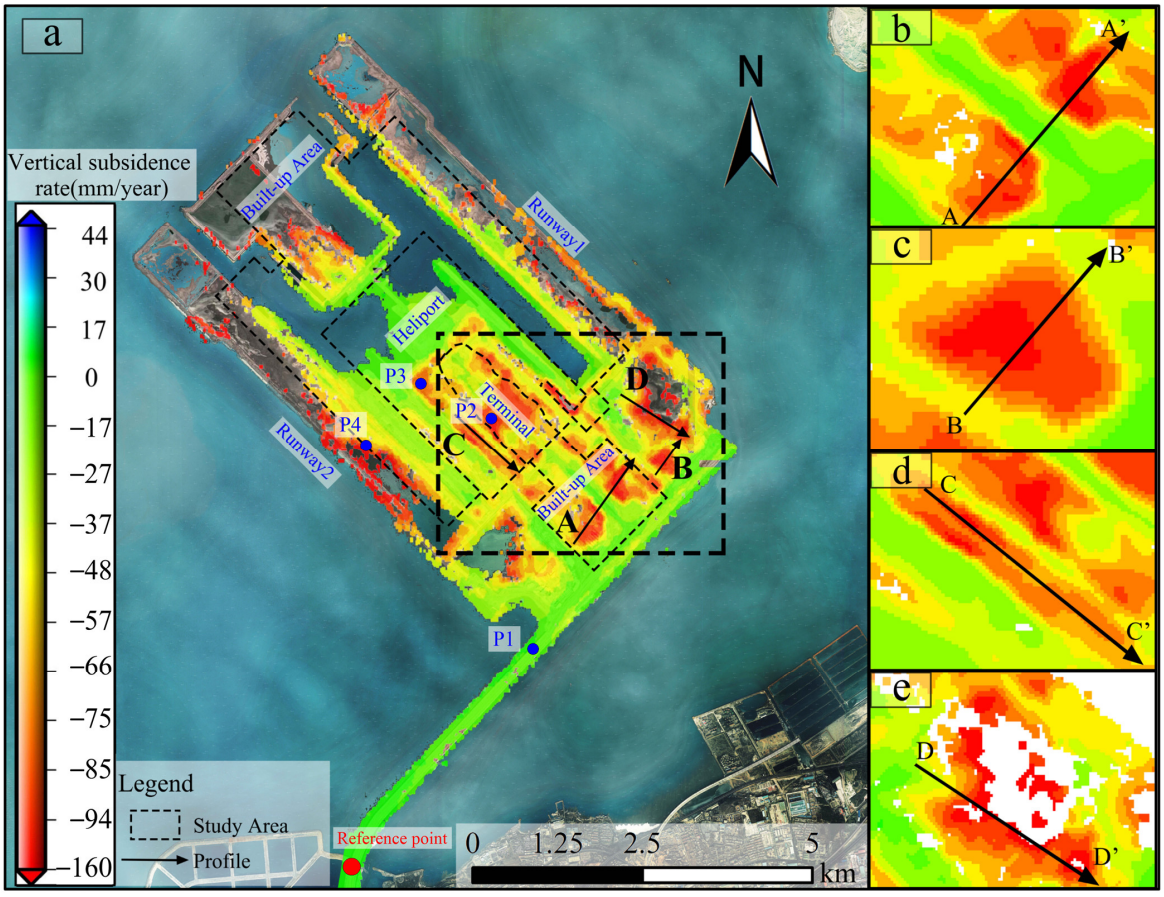

Figure 6. (**a**) Average annual vertical subsidence rate of Jinzhou Bay International Airport; (**b**–**e**) Subsidence rate along profiles AA′, BB′, CC′, and DD′, respectively; The blue points P1, P2, P3, and P4 in (**a**) were shown in Figure 8 with their accumulated subsidence; The red point in (**a**) denotes the reference point.

As shown in the spatial distribution of subsidence, most areas of the reclamation area are undergoing significant subsidence. From the vertical subsidence results in Figure 6a after ascending orbit decomposition, it can be seen that during the monitoring period from March 2017 to April 2021, some areas of the airport, such as the runway, terminal, and heliport areas of the airport are in a severe subsidence. It is revealed from the combination of Figures 6a and 8 that the accumulation of subsidence in the terminal was over 300 mm and the maximum vertical subsidence rate reached −160 mm/year. Moreover, the time series of subsidence areas in Figure 8 was near linear in the short term, but the subsidence rate was highly associated with the backfilling time, i.e., the longer the reclaimed time, the lower the subsidence rate.

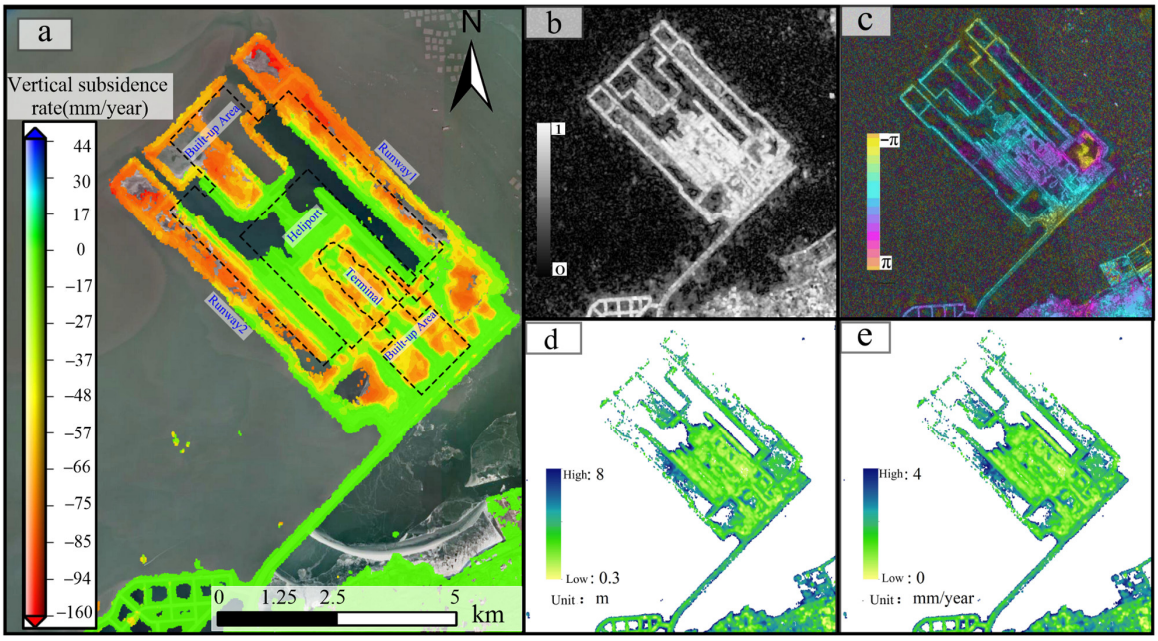

Figure 7. (**a**) Average annual subsidence rate distribution derived from descending track; (**b**) Average coherence coefficient diagram; (**c**) Differential interferogram (20200817–20200910); (**d**) Distribution of elevation residuals; (**e**) The error map of mean velocity results.

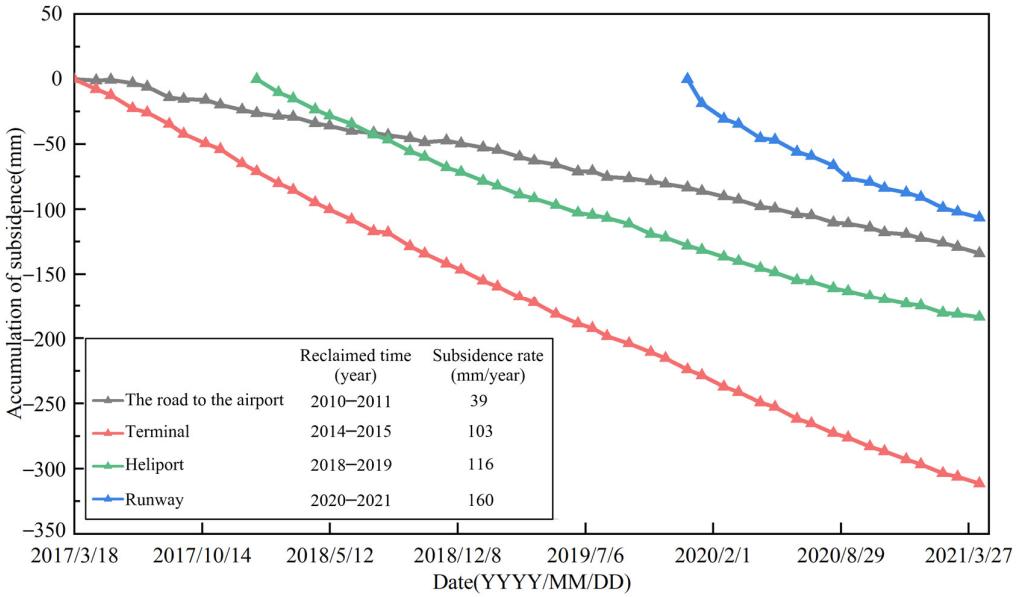

Figure 8. The accumulation subsidence in different areas of the airport. The location of P1–P4 were shown in Figure 6.

In order to further reveal the vertical ground subsidence spatial difference in DJBIA, four typical vertical subsidence areas with complete data, obvious vertical subsidence, and belonging to different reclamation stages were taken for vertical subsidence rate analysis. Figure 6b–e show these four more severe subsidence areas and selected profile lines AA′–DD′, respectively, and the corresponding four average annual vertical subsidence rate profile lines are shown in Figure 9a–d. Ground subsidence can be observed in all four profile line graphs, and there are inconsistent patterns in the curves of the subsidence areas for different reclamation periods and differences in the magnitude of ground subsidence.

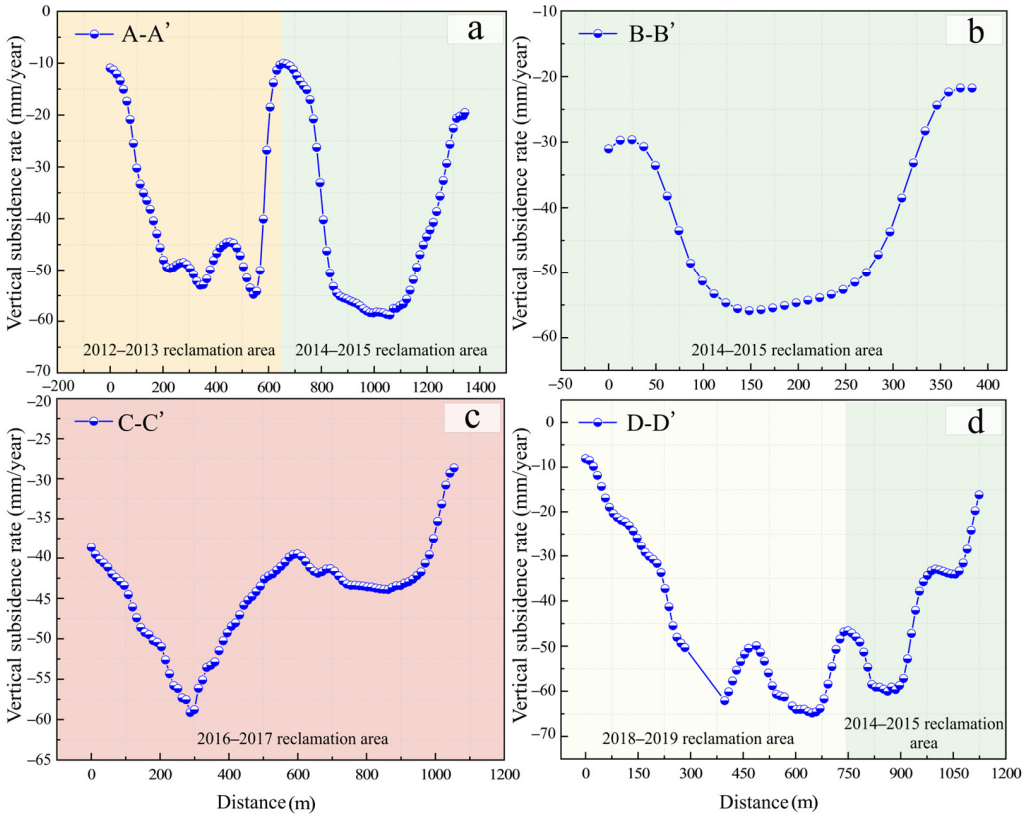

Figure 9. Vertical subsidence rate profiles (the location of the profile are marked in Figure 6). (**a**–**d**) profiles along AA′, BB′,CC′, DD′, respectively.

As shown in Table 3, the earlier the time of reclamation, the lower the vertical subsidence rate. In Figure 9, the different periods of completed reclamation are indicated by the colors corresponding to the periods of reclamation in Figure 2, where two different periods of reclamation are included in Figure 9a,d, respectively. By quantitatively analyzing the correlation between different reclamation periods and ground subsidence, it is found that the dividing line of the drastic change in the vertical subsidence rate coincides with the boundary of reclamation in different periods. The ground subsidence magnitude in the reclaimed area of DJBIA is closely related to its reclamation completion time, which means that significant subsidence occurred in the area where the reclamation was completed in the recent period, and the rate of subsidence decreases with time. This subsidence pattern is more consistent with the subsidence patterns of other offshore reclamation areas, for instance, the Hong Kong Chek Lap Kok Airport [14] and Shanghai Lingang New City, China [15].

The areas with vertical subsidence rates greater than −100 mm/year at DJBIA are located in the corner locations at the airport with the edge locations, which is in the reclamation areas completed in 2018–2019 and 2020–2021. The reclamation of the middle area of the airport was completed in 2012–2013 and 2014–2015, and its vertical subsidence rate was smaller but reached −70 mm/year to −80 mm/year. Overall, the vertical subsidence

rate exhibits an emission-like progression from the middle to the edge regions. There is a certain pattern of vertical subsidence rate in the areas where reclamation was completed at different periods. From Figure 10, it can be seen that the maximum, minimum, and median values of vertical subsidence rate are in different reclamation periods. The red points indicate the average vertical subsidence rate. The InSAR subsidence monitoring points in Figure 10 mean that the subsidence rate on the InSAR high-coherence points in Figure 6 shown by counting the magnitude of the rate, and the arcs next to the subsidence points represent the normal distribution curves of these points. The data of this figure are the same as shown in Figure 6 but they are shown in another way to reveal the relationship between reclamation time and vertical subsidence rate. The figure shows that the average vertical subsidence rate of the main body of the airport is: 2020–2021 reclamation area (−80 mm/year) > 2018–2019 reclamation area (−76 mm/year) > 2016–2017 reclamation area (−74 mm/year) > 2014–2015 reclamation area (−66 mm/year) > 2012–2013 reclamation area (−31 mm/year), which shows that the more recent the reclamation completion time is, the greater the average vertical subsidence rate is.

Table 3. Subsidence rate of profile in different periods.

Profile Name	Reclamation Time (Year)		Maximum Subsidence Rate (mm/Year)	
AA′	2012–2013	2014–2015	−91	−97
BB′	2014–2015		−93	
CC′	2016–2017		−99	
DD′	2018–2019	2014–2015	−108	−98

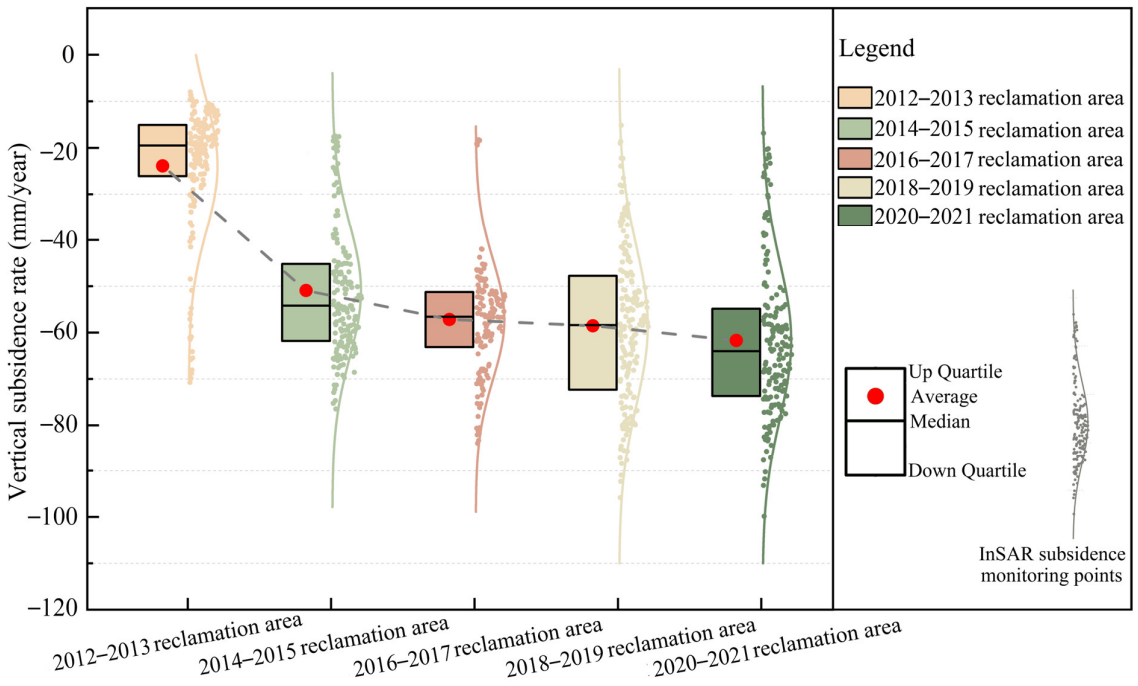

Figure 10. Temporal distribution of average vertical subsidence rates in different reclamation areas.

4.2. Terzaghi Consolidation Theory Verification and Prediction

The process stages of land reclamation are coast reclamation, blowing, subsidence, and soft foundation treatment, in which subsidence is an inevitable problem of land reclamation. This subsidence is a characteristic of subsidence exhibited by the compaction of the reclaimed soil layer, which generally tends to stabilize in value after more than 20 years [47]. During this time, the ground will continue to subsidence to different degrees. The ground subsidence related to land reclamation is primarily induced by three main mechanisms, which include the initial consolidation of alluvial clay deposits after land

reclamation, the secondary compression of alluvial clay deposits after land reclamation in the long term, and the creep of the fill-in land reclamation [24,26,48,49]. In particular, the initial consolidation of the filling soil in land reclamation accounts for the largest proportion of the total subsidence, which is generally more than 70% in the case of airports in land reclamation [14,50]. Moreover, the subsidence process of secondary compression and filling creep is much slower than the subsidence process of initial consolidation [24]. Terzaghi consolidation theory can provide an excellent explanation for this phenomenon.

From Figure 11, the subsidence rates of different reclamation area subsidence points in the reclamation area of DJBIA are taken during the period from March 2017 to April 2021. The subsidence points of the reclamation area in 2012–2013, 2014–2015, 2016–2017, 2018–2019, and 2020–2021 are indicated by orange, light green, light red, light yellow, and dark green points, respectively. The overall subsidence is undergoing the most significant rapid subsidence phase after the reclamation is completed.

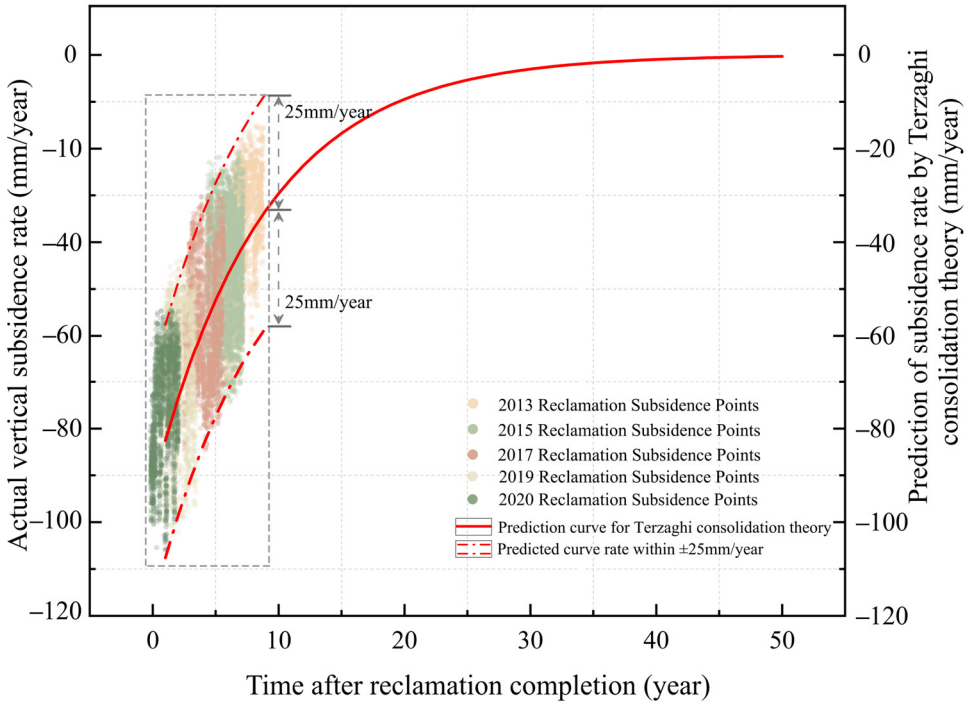

Figure 11. Prediction based on Terzaghi consolidation theory.

Based on the Terzaghi consolidation theory and combined with certain geological sampling data, such as permeability coefficient, initial pore ratio, and compression coefficient of DJBIA [30–32], the subsidence prediction curve of the area is obtained as shown in the red curve. As shown in Figure 11, the red prediction curve obtained by combining the geological parameters of the area with the Terzaghi consolidation theory shows that the reclamation area of the area in 2020 has an annual average vertical subsidence rate of about 82 mm/year in the first year, and the results of InSAR monitoring reveal that the first two years of vertical subsidence are within the range of 80 ± 25 mm/year, which is highly consistent with each other. Additionally, the trend of decreasing deformation in the following years is also highly consistent. The predicted subsidence in the reclaimed area in 2013 was around 32 mm/year, and the real subsidence was about 30 ± 25 mm/year, which confirmed the applicability and feasibility of the Terzaghi consolidation theory and the corresponding parameters used in this paper at Jinzhou Bay Airport. Meanwhile, the results not only show the entire airport is currently in a more significant and rapid subsidence phase, but also the vertical subsidence rate of the airport reclamation area is gradually slowing down over time. In addition, the future vertical subsidence rate of the newly reclaimed area in the region is about 80 ± 25mm/year, and the subsidence rate will gradually slow

down with the accumulation of reclamation time, and the vertical subsidence rate will slow down to about 30 ± 25mm/year after 10 years. It is demonstrated that this theory can provide an important reference to the prediction of land reclamation subsidence.

5. Conclusions

In this study, the time-series subsidence results of DJBIA from 2017–2021 were obtained by using the SBAS-InSAR technology based on 50 Sentinel-1A ascending images, and the Terzaghi consolidation theory was integrated to predict the future subsidence of DJBIA in time series. The prediction based on the current stage can generally identify the subsidence rate and trend in the study area, which is important for the control of the current and future construction. The main findings of this paper are listed in the following.

(1) Extensive and significant uneven ground subsidence is occurring throughout the land reclamation area of the airport, especially in the runway, terminal, and building areas, with the maximum subsidence rate exceeding −100 mm/year. By analyzing the maximum subsidence rate in four typical areas and the average regional subsidence rate in six different reclamation periods, it shows that there is a large connection between the ground subsidence rate and the reclamation time in this area, which means that the earlier the reclamation completion, the larger the subsidence rate.

(2) Based on Terzaghi consolidation theory and on-site geological parameters, a predicted subsidence rate curve was derived for the area, which was in high agreement with the InSAR monitored subsidence results in 2017–2021, verifying the applicability of the proposed prediction model based on Terzaghi consolidation theory for this land reclamation airport.

(3) The prediction model reveals that subsidence in the entire reclamation area is in a relatively significant and rapid stage at this stage, and the overall subsidence rate of the reclamation area will be decreasing dramatically as time goes by. The subsidence in the newly reclaimed area in the first two years is within the range of 80 ± 25 mm/year, and it will slow down to about 30 ± 25mm/year after 10 years.

Author Contributions: X.S. and C.C. implemented a combination of both methods. C.C. wrote the draft manuscript. K.D. supervised the experimental analysis and revised the manuscript. J.D., N.W., Y.Y. and X.D. made contributions on the experimental analysis. All authors have read and agreed to the published version of the manuscript.

Funding: This research was funded by the National Natural Science Foundation of China (Grant No. 41941019; No. 42072306; No. 41801391), State Key Laboratory of Geohazard Prevention and Geoenvironment Protection Independent Research Project (SKLGP2020Z012) and the fellowship of China Postdoctoral Science Foundation (2020M673322).

Conflicts of Interest: The authors declare no conflict of interest.

References

1. Cigna, F.; Tapete, D. Urban growth and land subsidence: Multi-decadal investigation using human settlement data and satellite InSAR in Morelia, Mexico. *Sci. Total Environ.* **2022**, *811*, 152211. [CrossRef] [PubMed]
2. Ma, P.; Wang, W.; Zhang, B.; Wang, J.; Shi, G.; Huang, G.; Chen, F.; Jiang, L.; Lin, H. Remotely sensing large- and small-scale ground subsidence: A case study of the Guangdong–Hong Kong–Macao Greater Bay Area of China. *Remote Sens. Environ.* **2019**, *232*, 111282. [CrossRef]
3. Hu, L.; Dai, K.; Xing, C.; Li, Z.; Tomás, R.; Clark, B.; Shi, X.; Chen, M.; Zhang, R.; Qiu, Q.; et al. Land subsidence in Beijing and its relationship with geological faults revealed by Sentinel-1 InSAR observations. *Int. J. Appl. Earth Obs. Geoinf.* **2019**, *82*, 101886. [CrossRef]
4. Aimaiti, Y.; Yamazaki, F.; Liu, W. Multi-Sensor InSAR Analysis of Progressive Land Subsidence over the Coastal City of Urayasu, Japan. *Remote Sens.* **2018**, *10*, 1304. [CrossRef]
5. Marshall, C.; Large, D.J.; Athab, A.; Evers, S.L.; Sowter, A.; Marsh, S.; Sjögersten, S. Monitoring tropical peat related settlement using ISBAS InSAR, Kuala Lumpur International Airport (KLIA). *Eng. Geol.* **2018**, *244*, 57–65. [CrossRef]
6. Jiang, H.; Balz, T.; Cigna, F.; Tapete, D. Land Subsidence in Wuhan Revealed Using a Non-Linear PSInSAR Approach with Long Time Series of COSMO-SkyMed SAR Data. *Remote Sens.* **2021**, *13*, 1256. [CrossRef]

7. Ramirez, R.A.; Lee, G.-J.; Choi, S.-K.; Kwon, T.-H.; Kim, Y.-C.; Ryu, H.-H.; Kim, S.; Bae, B.; Hyun, C. Monitoring of construction-induced urban ground deformations using Sentinel-1 PS-InSAR: The case study of tunneling in Dangjin, Korea. *Int. J. Appl. Earth Obs. Geoinf.* **2022**, *108*, 102721. [CrossRef]
8. Dai, K.; Li, Z.; Xu, Q.; Bürgmann, R.; Milledge, D.G.; Tomas, R.; Fan, X.; Zhao, C.; Liu, X.; Peng, J.; et al. Entering the era of earth observation-based landslide warning systems: A novel and exciting framework. *IEEE Geosci. Remote Sens. Mag.* **2020**, *8*, 136–153. [CrossRef]
9. Shi, X.; Yang, C.; Zhang, L.; Jiang, H.; Liao, M.; Zhang, L.; Liu, X. Mapping and characterizing displacements of active loess slopes along the upstream Yellow River with multi-temporal InSAR datasets. *Sci. Total Environ.* **2019**, *674*, 200–210. [CrossRef]
10. Fan, X.; Xu, Q.; Scaringi, G.; Dai, L.; Li, W.; Dong, X.; Zhu, X.; Pei, X.; Dai, K.; Havenith, H.-B. Failure mechanism and kinematics of the deadly June 24th 2017 Xinmo landslide, Maoxian, Sichuan, China. *Landslides* **2017**, *14*, 2129–2146. [CrossRef]
11. Tomás, R.; Li, Z.; Lopez-Sanchez, J.M.; Liu, P.; Singleton, A. Using wavelet tools to analyse seasonal variations from InSAR time-series data: A case study of the Huangtupo landslide. *Landslides* **2016**, *13*, 437–450. [CrossRef]
12. Wasowski, J.; Bovenga, F. Investigating landslides and unstable slopes with satellite Multi Temporal Interferometry: Current issues and future perspectives. *Eng. Geol.* **2014**, *174*, 103–138. [CrossRef]
13. Jiang, Y.; Liao, M.; Wang, H.; Zhang, L.; Balz, T. Deformation Monitoring and Analysis of the Geological Environment of Pudong International Airport with Persistent Scatterer SAR Interferometry. *Remote Sens.* **2016**, *8*, 1021. [CrossRef]
14. Jiang, L.; Lin, H. Integrated analysis of SAR interferometric and geological data for investigating long-term reclamation settlement of Chek Lap Kok Airport, Hong Kong. *Eng. Geol.* **2010**, *110*, 77–92. [CrossRef]
15. Pepe, A.; Bonano, M.; Zhao, Q.; Yang, T.; Wang, H. The Use of C-/X-Band Time-Gapped SAR Data and Geotechnical Models for the Study of Shanghai's Ocean-Reclaimed Lands through the SBAS-DInSAR Technique. *Remote Sens.* **2016**, *8*, 911. [CrossRef]
16. Zhao, Q.; Lin, H.; Gao, W.; Zebker, H.A.; Chen, A.; Yeung, K. InSAR detection of residual settlement of an ocean reclamation engineering project: A case study of Hong Kong International Airport. *J. Oceanogr.* **2011**, *67*, 415–426. [CrossRef]
17. Dai, K.; Shi, X.; Gou, J.; Hu, L.; Chen, M.; Zhao, L.; Dong, X.; Li, Z. Diagnosing Subsidence Geohazard at Beijing Capital International Airport, from High-Resolution SAR Interferometry. *Sustainability* **2020**, *12*, 2269. [CrossRef]
18. Gao, M.; Gong, H.; Chen, B.; Zhou, C.; Chen, W.; Liang, Y.; Shi, M.; Si, Y. InSAR time-series investigation of long-term ground displacement at Beijing Capital International Airport, China. *Tectonophysics* **2016**, *691*, 271–281. [CrossRef]
19. Lu, M.; Deng, K.; Feng, G.; Li, K.; Xiong, Z.; Wang, Y.; He, S. Reclaimed-Airport Surface-Deformation Monitoring by Improved Permanent-Scatterer Interferometric Synthetic-Aperture Radar: A Case Study of Shenzhen Bao'an International Airport, China. *Photogramm. Eng. Remote Sens.* **2021**, *87*, 105–116.
20. Liu, P.; Chen, X.; Li, Z.; Zhang, Z.; Xu, J.; Feng, W.; Wang, C.; Hu, Z.; Tu, W.; Li, H. Resolving surface displacements in Shenzhen of China from time series InSAR. *Remote Sens.* **2018**, *10*, 1162. [CrossRef]
21. Susaki, J.; Tsujino, M.; Anahara, T. Fusion of different frequency SAR images for DInSAR-based land subsidence monitoring. In Proceedings of the 2017 IEEE International Geoscience and Remote Sensing Symposium (IGARSS), Worth, TX, USA, 23–28 July 2017; pp. 945–948.
22. Ito, H.; Susaki, J.; Anahara, T. Integrating multi-temporal sar images and gps data to monitor three-dimensional land subsidence. *ISPRS Ann. Photogramm. Remote Sens. Spat. Inf. Sci.* **2019**, *4*, 9–16. [CrossRef]
23. Ito, H.; Susaki, J. Land subsidence monitoring by integrating PSI and Geodetic Deformation Measurements. In Proceedings of the IGARSS 2018-2018 IEEE International Geoscience and Remote Sensing Symposium, Valencia, Spain, 23–27 July 2018; pp. 498–501.
24. Xu, B.; Feng, G.; Li, Z.; Wang, Q.; Wang, C.; Xie, R. Coastal Subsidence Monitoring Associated with Land Reclamation Using the Point Target Based SBAS-InSAR Method: A Case Study of Shenzhen, China. *Remote Sens.* **2016**, *8*, 652. [CrossRef]
25. Zhuo, G.; Dai, K.; Huang, H.; Li, S.; Shi, X.; Feng, Y.; Li, T.; Dong, X.; Deng, J. Evaluating Potential Ground Subsidence Geo-Hazard of Xiamen Xiang'an New Airport on Reclaimed Land by SAR Interferometry. *Sustainability* **2020**, *12*, 6991. [CrossRef]
26. Liu, X.; Zhao, C.; Zhang, Q.; Yang, C.; Zhang, J. Characterizing and monitoring ground settlement of marine reclamation land of Xiamen New Airport, China with Sentinel-1 SAR Datasets. *Remote Sens.* **2019**, *11*, 585. [CrossRef]
27. Guo, F.; Zhang, H.; Fan, Y.; Zhu, P.; Wang, S.; Lu, X.; Jin, Y. Environment. Detection and evaluation of a ventilation path in a mountainous city for a sea breeze: The case of Dalian. *Build. Environ.* **2018**, *145*, 177–195. [CrossRef]
28. Zhu, X. Research on Risk Assessment and Disaster Mitigation of Geological Disasters in Dalian. Master's Thesis, Liaoning Normal University, Liaoning, China, 2021.
29. China Civil Aviation Website. Dong Zhiyi went to Dalian New Airport for Research. Available online: http://www.caacnews.com.cn/1/1/201911/t20191107_1285087_wap.html. (accessed on 1 April 2022).
30. Bai, W. Improved Algorithm and Application of One-Dimensional Consolidation Theory for Soft Soil Foundation. Master's Thesis, Xi'an University of Technology, Xi'an, China, 2020.
31. Deng, H. Study on Reclamation and Soft Soil Characteristics in Dalian Coastal Zone. Master's Thesis, Jilin University, Jilin, China, 2020.
32. Cong, B. Calculation of the Foundation Settlement of Soft Clay at the DaLian Offshore Airport. Master's Thesis, Dalian University of Technology, Dalian, China, 2013.
33. Lanari, R.; Mora, O.; Manunta, M.; Mallorquí, J.J.; Berardino, P.; Sansosti, E. A small-baseline approach for investigating defor-mations on full-resolution differential SAR interferograms. *IEEE Trans. Geosci. Remote Sens.* **2004**, *42*, 1377–1386. [CrossRef]

34. Osmanoğlu, B.; Sunar, F.; Wdowinski, S.; Cabral-Cano, E. Time series analysis of InSAR data: Methods and trends. *ISPRS J. Photogramm. Remote Sens.* **2016**, *115*, 90–102. [CrossRef]
35. Costantini, M. A novel phase unwrapping method based on network programming. *IEEE Trans. Geosci. Remote Sens.* **1998**, *36*, 813–821. [CrossRef]
36. Hooper, A.; Zebker, H.A. Phase unwrapping in three dimensions with application to InSAR time series. *JOSA A* **2007**, *24*, 2737–2747. [CrossRef]
37. Chen, G.; Zhang, Y.; Zeng, R.; Yang, Z.; Chen, X.; Zhao, F.; Meng, X. Detection of land subsidence associated with land crea-tion and rapid urbanization in the chinese loess plateau using time series insar: A case study of Lanzhou new district. *Remote Sens.* **2018**, *10*, 270. [CrossRef]
38. Liao, M.; Wang, T. *Time Series InSAR Technology and Application*; Science Press: Beijing, China, 2014; pp. 83–86.
39. Goldstein, R.M.; Werner, C. Radar interferogram filtering for geophysical applications. *Geophys. Res. Lett.* **1998**, *25*, 4035–4038. [CrossRef]
40. Dai, K.; Liu, G.; Li, Z.; Li, T.; Yu, B.; Wang, X.; Singleton, A. Extracting Vertical Displacement Rates in Shanghai (China) with Multi-Platform SAR Images. *Remote Sens.* **2015**, *7*, 9542–9562. [CrossRef]
41. Wang, H.; Wright, T.J.; Yu, Y.; Lin, H.; Jiang, L.; Li, C.; Qiu, G. InSAR reveals coastal subsidence in the Pearl River Delta, China. *Geophys. J. Int.* **2012**, *191*, 1119–1128. [CrossRef]
42. Huang, J.; Griffiths, D.J.G. One-dimensional consolidation theories for layered soil and coupled and uncoupled solutions by the finite-element method. *Geotechnique* **2010**, *60*, 709–713. [CrossRef]
43. Chen, Z. *Soil Mechanics*; Tsinghua University Press: Beijing, China, 2006; pp. 100–160.
44. Barnes, G. *Soil Mechanics: Principles and Practice*; Macmillan International Higher Education: London, UK, 2016.
45. Terzaghi, K.; Peck, R.B.; Mesri, G. *Soil Mechanics in Engineering Practice*; John Wiley and Sons: Hoboken, NJ, USA, 1996; pp. 1–592.
46. Dai, K.; Liu, G.; Yu, B.; Jia, H.; Ma, D.; Wang, X. Detecting Subsidence along a High Speed Railway by Ultrashort Baseline TCP-InSAR with High Resolution Images. *Int. Arch. Photogramm. Remote Sens. Spat. Inf. Sci.* **2013**, *XL-7/W2*, 61–65. [CrossRef]
47. Wang, Q.; Zhang, Y.; Dong, Y.; Fu, Y. Subsidence monitoring of land reclamation area dike project based on time-series InSAR technology. *Highway* **2021**, *66*, 276–281.
48. Tosen, R.; Pickles, A.; Jaros, M. Assessment of differential settlement at Chek Lap Kok Airport reclamation site. In *Proceedings of the a Seminar on the Geotechnical Aspects of the Airport Core Projects*; Hong Kong Institution of Civil Engineers: Hong Kong, China, 1998.
49. Plant, G.W.; Covil, C.S.; Hughes, R.A. *Site Preparation for the New Hong Kong International Airport*; Thomas Telford: London, UK, 1998.
50. Pickles, A.; Tosen, R. Settlement of Reclaimed Land for the New Hong Kong International Airport. *Proc. Inst. Civ. Eng.-Geotech. Eng.* **1998**, *131*, 191–209. [CrossRef]